Journal of
Composites Science

MDPI

Article

Synthesis of Conjugates of PEG-RGD Derivatives with Fe_3O_4 Magnetic Nanoparticles for Cell Labelling

Alexander M. Demin [1,*], Alexander V. Vakhrushev [1], Alexandra G. Pershina [2,3], Alexandra A. Syomchina [2], Lina V. Efimova [2], Maksim S. Karabanalov [4], Mikhail A. Uimin [5], Iliya V. Byzov [5], Artem S. Minin [5] and Victor P. Krasnov [1]

[1] Postovsky Institute of Organic Synthesis, Russian Academy of Sciences (Ural Branch), Ekaterinburg 620990, Russia; avv@ios.uran.ru (A.V.V.); ca@ios.uran.ru (V.P.K.)
[2] Center of Bioscience and Bioengineering, Siberian State Medical University, Tomsk 634050, Russia; allysyz@mail.ru (A.G.P.); sonjochek@mail.ru (A.A.S.); efimova.lina@gmail.com (L.V.E.)
[3] Research School of Chemistry & Applied Biomedical Sciences, National Research Tomsk Polytechnic University, Tomsk 634050, Russia
[4] Institute of New Materials and Technologies, Ural Federal University, Ekaterinburg 620002, Russia; maks_s_k@mail.ru
[5] Mikheev Institute of Metal Physics, Russian Academy of Sciences (Ural Branch), Ekaterinburg 620990, Russia; uimin@imp.uran.ru (M.A.U.); ivbyzov@gmail.com (I.V.B.); calamatica@gmail.com (A.S.M.)
* Correspondence: amd2002@mail.ru

Abstract: The purpose of this research is to design nanocomposite materials for biomedical applications. New conjugates of PEG derivatives of RGD peptides and magnetic nanoparticles, based on Fe_3O_4 (MNPs) with silica coating covalently labelled with fluorescent dye Cyanine5, were obtained. It was shown that a higher loading level of RGD peptides occurred in the case of MNPs with SiO_2/aminopropylsilane coating, synthesised using *N*-(phosphonomethyl)iminodiacetic acid (PMIDA) as a surfactant. To confirm the structure and chemical purity of the new RGD-PEG conjugate, a number of methods were used, including ^{1}H NMR, HRMS, and RP-HPLC. The characterisation of MNPs was carried out using the following physical methods: TEM, FTIR, EDX, CHN analysis, DLS, fluorescence spectrometry, vibration magnetometry, and relaxometry. Samples obtained from PMIDA-stabilised MNPs contained a greater amount of the peptide and possessed better hydrodynamic characteristics than samples obtained from non-stabilised MNPs. A comparative study of the MNP cytotoxicity was carried out towards 4T1 and MDA-MB231 cell lines (MTT test), and the possibility of cell labelling was assessed. The cellular uptake was more efficient for nanoconjugates obtained without PMIDA. The data obtained can be used for the design of materials for cell labelling and visualisation.

Keywords: magnetic nanoparticles; Fe_3O_4; RGD peptide synthesis; nanoconjugates; Cyanine5; cell labelling

Citation: Demin, A.M.; Vakhrushev, A.V.; Pershina, A.G.; Syomchina, A.A.; Efimova, L.V.; Karabanalov, M.S.; Uimin, M.A.; Byzov, I.V.; Minin, A.S.; Krasnov, V.P. Synthesis of Conjugates of PEG-RGD Derivatives with Fe_3O_4 Magnetic Nanoparticles for Cell Labelling. *J. Compos. Sci.* **2024**, *8*, 486. https://doi.org/10.3390/jcs8120486

Academic Editors: José António Covas, Yanshuai Wang and Giuseppe Cavallaro

Received: 1 October 2024
Revised: 22 October 2024
Accepted: 20 November 2024
Published: 22 November 2024

1. Introduction

Currently, magnetic nanoparticles (MNPs) are actively applied in the development of multimodal systems used in various medical and biological approaches [1–4], such as therapy [5–9] and cancer diagnostics using MRI, MPI, etc. [10–13], cell labelling, including implementation of cell tracking, visualisation [14–16], sorting [17–19], as well as other biological engineering approaches.

Often, to increase the efficiency of accumulation of such nanoconjugates in tumour cells and tissues, targeting peptide molecules are introduced into their composition [20–22], in particular, the RGD peptides [23–27], which are known to be capable of specific binding with integrins $\alpha_V\beta_3$ and $\alpha_V\beta_5$, overexpressed on the tumour cell surface [28–30]. Dong X. et al. performed molecular dynamics simulations of the interaction of RGD peptides with

$\alpha_V\beta_3$ molecules and demonstrated specific binding sites involving the COOH group of L-aspartic acid in the protein and the guanidine group of L-arginine in the RGD peptide molecule [31]. This indicated that the guanidine group of the L-arginine in the peptides widely used in the nanomaterial design should remain free to ensure specific identification of integrins and, accordingly, to maintain the high efficiency of these nanomedicines. Therefore, an important task in the design of conjugates of RGD peptide derivatives is the development of an approach to regioselective binding of the peptide to the functional groups of the MNP surface, without the participation of the guanidine group of L-arginine in the synthesis. There are several approaches to the immobilisation of peptides and, in particular, RGD peptide derivatives on the surface of MNPs [32]. As a rule, covalent bonding of surface functional groups of MNPs with free functional groups of peptide derivatives is used for these purposes, for example, due to an amide bond formation between the COOH and NH_2 groups [24–27], a thioether bond formation as a result of the reaction of the maleimide group with the mercapto group [33–37], or through the Cu^{2+}-catalysed cycloaddition of azides with terminal alkynes ("click chemistry") [23].

It is known that poly(ethylene glycol) (PEG) molecules provide additional stabilisation of colloidal solutions of nanoparticles, as well as a "stealth effect" in relation to the monocyte–macrophage system in the case of introducing particles into the bloodstream, and they are used in the design of modern nano-formulations [38,39]. Therefore, PEG molecules are often used as linkers in nanomaterials based on MNPs and peptides. Thus, in [24], a conjugate of thiolated RGD peptides with a bifunctional PEG molecule containing a maleimide and amino group at the ends was synthesised. It was then used to modify the surface of sodium-citrate-stabilised MNPs. In another work [33], on the contrary, the surface of MNPs was first modified with diphosphate-PEG molecules containing a maleimide group, and then conjugation with thiolated RGD peptides was carried out. In [37], SiO_2-covered MNPs with a PEG coating were similarly conjugated with c(RGDfC) due to nucleophilic addition of the L-cysteine thiol group of RGD peptides to the maleimide moiety of PEG.

In order to obtain new materials of interest for the development of cancer diagnostic tools using MRI or for tumour cell labelling, a convenient approach to conjugation of RGD peptides with MNPs via PEG-linkage is proposed. For this purpose, a novel PEG-containing derivative of RGD peptides was obtained, which was then covalently fixed on the surface of Fe_3O_4 MNPs coated with SiO_2. It is known that the use of surfactants before applying SiO_2 significantly affects the properties of the coating. It increases the coating area and the number of active centres on it, which leads to an improvement in the efficiency of immobilisation of organic molecules on the resulting material [36]. Therefore, in this work, a comparison of the loading level of PEG derivatives of RGD peptides on nanoparticles obtained without surfactants, using *N*-(phosphonomethyl)iminodiacetic acid (PMIDA), was carried out. Additional objectives of the study were to investigate the in vitro cytotoxicity of synthesised MNPs and to assess the possibility of cell labelling.

2. Materials and Methods

2.1. Materials

$FeSO_4 \cdot 7H_2O$ and $FeCl_3 \cdot 6H_2O$ (Sigma-Aldrich, St. Louis, MO, USA), (3-aminopropyl)-trimethoxysilane (APTMS; Alfa Aesar, Heysham, Lancashire, UK), tetraethoxysilane (TEOS; Alfa Aesar, Heysham, Lancashire, UK), *N*-(phosphonomethyl)iminodiacetic acid (PMIDA; Sigma-Aldrich, St. Louis, MO, USA), *O*-[carboxypropyl]-*O*′-[3-(N-hydroxysuccinimidyloxy)-3-oxopropyl]pentacosaethylene glycol (PEG-NHS; Quanta Biodesign, Plain city, OH, USA), and di-*tert*-butyl (L,L)-(N^{α}-4-carboxybutanoyl-N^{ω}-Pbf-arginyl)-glycyl-aspartate (Arg(Pbf)-GlyAsp(OBu^t)$_2$) [40,41] were used.

2.2. Synthesis of MNPs

2.2.1. Synthesis of Initial Nanoparticles (MNPs **1** and **2**)

A saturated solution of $NH_3 \cdot H_2O$ (6 mL) was infused to 50 mL of an aqueous solution of $FeCl_3 \cdot 6H_2O$ (1167.4 mg, 4.32 mmol) and $FeSO_4 \cdot 7H_2O$ (600.4 mg, 2.16 mmol) at 40 °C (in accordance with [36]). After 10 min of stirring, the MNPs **1** were collected using a permanent magnet, washed with distilled water (3 × 40 mL), and diluted with water up to 50 mL. Then, MNPs **1** were modified with PMIDA (as described in [36]): 30 mL of PMIDA solution (26.5 mg, 0.117 mmol) in distilled water was infused to 25 mL of colloidal solution of MNPs **1** (270 mg, 1.166 mmol) at 40 °C. After 4 h of stirring at 40 °C and incubating for another 16 h at 20 °C, MNPs **2** (55 mL, 5.45 mg/mL) were obtained.

2.2.2. Application of SiO_2 Coating on MNPs (MNPs **3**–**5**) and Their Aminopropylsilane Functionalisation (MNPs **6** and **7**)

Colloidal solutions of MNPs **1** or **2** (0.245 g) in water (50 mL) were diluted with EtOH (125 mL) and heated up to 40 °C. Thereafter, a solution of TEOS (355 µL, 1.59 mmol) in EtOH (10 mL) was infused and a saturated solution of $NH_3 \cdot H_2O$ (3.5 mL) was introduced drop-by-drop over 10 min [36]. Stirring was continued for 4 h at 40 °C and for another 16 h at 20 °C. MNPs were precipitated in a centrifuge at 40,000× *g* for 30 min and washed with distilled water (3 × 60 mL) until a neutral reaction occurred. The obtained MNPs were suspended in 30 mL of H_2O, and colloidal solutions of MNPs-SiO_2 **3** (9.67 mg/mL) or MNPs-SiO_2 **4** (8.48 mg/mL), respectively, were obtained. The resulting MNPs-SiO_2 **3** and **4** were functionalised with APTMS. A solution of APTMS (3 mmol per 1 g of nanoparticles) in EtOH (20 mL) was introduced dropwise to a suspension of 170 mg of MNPs-SiO_2 (**3** or **4**) in 115 mL of EtOH 70% at 40 °C. After 4 h of stirring at 40 °C and for another 16 h at 20 °C, modified MNPs were collected using a permanent magnet, washed with EtOH (50 mL), water (2 × 50 mL), and MeCN (2 × 50 mL), and suspended in dry MeCN (20 mL). As a result, colloidal solutions of MNPs-SiO_2-APS **5** (8.62 mg/mL) and **6** (9.56 mg/mL) were obtained.

2.2.3. Synthesis of PEG-RGD Conjugate **6**

NHS-PEG(25)-COOH (PEG-NHS; 100 mg, 0.076 mmol) and Arg(Pbf)GlyAsp(OBu^t)$_2$ (RGD; 54.1 mg, 0.076 mmol) were dissolved in 10 mL of dry CH_2Cl_2 and incubated for 24 h at 20 °C. The resulting product was purified by flash chromatography using a $CHCl_3$:EtOH system as an eluent with a gradient from 100:0 to 50:50. Then, 139.5 mg (96%) of a white powder of PEG-RGD conjugate **6** was obtained.

^{1}H NMR (500 MHz, DMSO): δ = 11.1–10.0 (br s, 1H (COOH)), 8.19 (t, *J* = 5.9 Hz, 1H (NH, Gly)), 8.14–8.06 (m, 2H (NH Asp, NH, Arg)), 4.49 (dt, *J* = 6.4, 6.8 Hz, 1H ($C^{\alpha}H$, Asp)), 4.20 (dt, *J* = 7.1, 6.8 Hz, 1H ($C^{\alpha}H$, Arg)), 3.70 (d, *J* = 5.9 Hz, 2H (CH_2, Gly)), 3.60 (t, *J* = 6.3 Hz, 2H (N–CO–CH_2, PEG)), 3.54–3.46 (m, 104H, PEG)), 3.02 (dt, *J* = 6.4, 6.3 Hz, 2H ($C^{\delta}H_2$, Arg)), 2.96 (s, 2H (CH_2, Pbf)), 2.64 (dd, *J* = 6.4, 16.3 Hz, 2H ($C^{\beta}H$, Asp)), 2.54 (dd, *J* = 6.9, 16.5 Hz, 2H ($C^{\beta}H_2$, Asp)), 2.48 (s, 3H (Aryl CH_3, Pbf)), 2.44 (t, *J* = 6.5 Hz, 2H (HOOC–CH_2, PEG)), 2.42 (s, 3H (Aryl CH_3, Pbf)), 2.01 (s, 3H (Aryl CH_3, Pbf)), 1.68–1.59 (m, 2H ($C^{\beta}H_2$, Arg)), 1.54–1.44 (m, 2H ($C^{\gamma}H_2$, Arg)), 1.41 (s, 6H (2CH_3, Pbf)), 1.39 (s, 9H (OBu^t, Asp)), 1.38 ppm (s, 9H (OBu^t, Asp)).

RP-HPLC (Kromasil 100-5 C18; 60% aqueous MeCN; 35 °C; 0.8 mL/min flow rate; detection at 220, 230, 260 nm): retention time 4.59 min.

HRMS (ESI-POS) *m*/*z* calculated for C87H159N6O37S $[M + H]^+$: 1912.0460; found: 1912.0444.

2.2.4. Conjugation of RGD with MNPs (MNPs-RGD **7**–**12**) General Procedure

To prepare solution A, HBTU (3.2 mg) and PEG-RGD (16.1 mg), taken in equimolar amounts (8.4 µmol), were dissolved in 2 mL of dry MeCN, and then DIPEA (59 µmol) was added. After 30 min, 1.25, 0.5, and 0.25 mL of solution A (containing 10, 4, and 2 mg of PEG-RGD, respectively) and dry MeCN were added to three flasks containing 20 mg of

MNPs-SiO_2-APS **5** (or MNPs-SiO_2-APS **6**) to a total volume of 5 mL in each parallel. The mixtures were sonicated for 15 s. Then, after 20 h, MNPs were precipitated on a permanent magnet, washed with deionised water 3 × 5 mL, and suspended in 2 mL of H_2O. The colloidal solutions of MNP-RGD **7**–**12** with a concentration of 10 mg/mL were obtained.

2.2.5. Synthesis of MNPs-RGD*TFA **13**–**18** General Procedure

MNPs from 1.0 mL of each sample of MNPs-RGD **7**–**12** colloidal solutions were precipitated on a permanent magnet, suspended in 1 mL of TFA 95%, sonicated for 15 s, and left for 3 h at 20 °C. MNPs were precipitated using a centrifuge (10,000× *g*, 10 min), washed with distilled water at 3 × 1 mL, and suspended in H_2O to obtain 1 mL of MNPs-RGD*TFA **13**–**18** colloidal solutions.

2.3. Characterisation of Synthesised Materials

To confirm the structure and chemical purity of the new RGD-PEG conjugate, a number of methods were used, including ^{1}H NMR, HRMS, and RP-HPLC.

NMR spectra of synthesised peptide derivatives and conjugate PEG-RGD were performed on a Bruker Avance 500 (500 MHz, Bruker, Karlsruhe, Germany). Reversed-phase HPLC was realised on an Agilent 1100 (Agilent Technologies, Santa Clara, CA, USA) with a Kromasil 100-5-C18 column (Nouryon, Göteborg, Sweden). High-resolution mass spectra (HRMS) were performed on a Bruker maXis impact HD instrument (Bruker, Karlsruhe, Germany).

The characterisation of MNPs was carried out using the following physical methods: TEM, FTIR, fluorescence spectrometry, EDX, CHN analysis, vibration magnetometry, DLS, and relaxometry.

TEM MNP studies were carried out on a Tecnai G2 30 (Thermo Fisher Scientific, Waltham, MA, USA). The IR spectra were recorded on a Perkin Elmer Spectrum Two FTIR spectrometer (Perkin Elmer, Waltham, MA, USA) equipped with the attenuated total reflection (ATR) accessory (for analysis, MNP sample powder was sprinkled onto a diamond crystal of the ATR accessory and analysed). Mass fractions of C, H, and N were determined using a CHN EuroEA 3000 automatic analyser (EuroVector Instruments and Software, Milan, Italy; the analysis was carried out in two repetitions). Mass fractions of Fe, Si, and P were determined using an EDX-7000 X-ray fluorescence spectrometer (Shimadzu, Kyoto, Japan; the analysis was carried out in two repetitions). Excitation and emission spectra of MNP aqueous colloidal solutions (0.1–0.2 mg/mL) were obtained using a Cary Eclipse fluorescence spectrometer (Agilent, Santa Clara, CA, USA). The magnetic properties of the MNP powders were studied on a magnetic vibromagnetometer with magnetic fields (*H*) of no more than 25 kOe.

DLS characterisation of aqueous colloidal solutions of synthesised MNPs (0.1–0.2 mg/mL) was performed on a Photocor Compact-Z instrument (Photocor, Moscow, Russia).

The relaxivities *r*1 and *r*2 of MNP colloidal solutions were found using a relaxometer (1 kOe, 4.31 MHz, echo 1 ms; ECOTEK Corporation, Houston, TX, USA).

2.4. In Vitro Experiments

To assess MNPs' cytotoxicity, the MTT assay was used. For this purpose, 4 × 10^3 4T1 cells (ATCC) or 8 × 10^3 MDA-MB231 cells (ECACC) were grown in the wells of a 96-well plate. A complete DMEM/F12 (Gibco, Grand Island, NY, USA) supplemented with 10% FBS (Gibco, Paisley, UK), 1× Glutamax (Gibco, Grand Island, NY, USA), and 1× PenStrep (Gibco, Grand Island, NY, USA) was used. On the next day, 10 µL of nanoparticles (suspended in water to a concentration of 500, 250, 125, or 62.5 µg/mL) was added to the cells, and the final volume in the wells was 100 µL. Before addition, the MNP suspension was sonicated. Instead of nanoparticles, 10 µL of 0.01% Triton X100 (PanReac, Barcelona, Spain) was added in the wells of the positive control, and 10 µL of sterile H_2O in the wells of the negative control. The cells were incubated with MNPs in a CO_2 incubator for 24 or 48 h. The MTT assay was performed as described in [8].

To study the uptake of nanoparticles by cells, 5×10^4 cells were grown in the wells of a 24-well plate in 450 µL of a complete DMEM/F12. The next day, 50 µL of nanoparticles (suspended in water to a concentration of 12.5 µg/mL) was added to the cells. Then, the plates were incubated in a CO_2 incubator. General (nonspecific) uptake was accessed in 4 h after MNPs' addition. To assess the specific uptake of MNPs due to binding to receptors on the cell surface, the incubation with nanoparticles was carried out on ice. Briefly, the plates with cells were preliminarily placed on ice for 30 min; after that, MNPs were added, and the plates were left on ice for 1 h. The medium was discarded, the cells were washed with cold PBS two times to completely remove MNPs, 500 µL of warm complete DMEM/F12 was added, and the cells were incubated for 4 h at 37 °C in a CO_2 incubator. To determine the efficiency of MNP uptake, the cells were dissociated from the plate surface using TrypLE (Gibco, Grand Island, NY, USA), resuspended in PBS, and analysed on a flow cytometer, Cytoflex (Beckman Coulter, Suzhou, China). For analysis, a cell population was gated on a two-parameter histogram of FSC-A versus SSC-A; then, doublets were excluded from the analysis on a histogram of SSC-A versus SSC-H. To exclude dead cells from the analysis, DAPI was used. Efficiency of MNP uptake was expressed as the percent of Cy5-positive cells among the population of live cells. For fluorescence microscopy analysis, cells were plated as described above on coverslips pre-coated with poly-L-Lys in a 24-well plate. The cells were incubated with MNPs for 4 or 24 h, then were washed, fixed using 4% paraformaldehyde, permeabilised (0.05% TritonX 100, PanReac, Barcelona, Spain), and stained using Phalloidin-Atto 488 (Thermo Fisher, Eugene, OR, USA). The coverslips were then removed from the wells and transferred to microscope slides. The mounting medium with DAPI—Aqueous, Fluoroshield (Abcam, Waltham, MA, USA)—was used for nuclei staining.

3. Results and Discussion

3.1. MNP Synthesis and Characterisation

In the present study, we used Fe_3O_4-based MNPs synthesised by the coprecipitation method. For SiO_2 coating (Scheme 1), we used both the bare MNPs **1** and **2** stabilised with PMIDA, similar to [12,36]. Silanes were covalent-fixed on the surface of Fe_3O_4 MNPs due to Fe–O–Si bond formation [42]. This can be confirmed by the presence of absorption bands in the IR spectra in the region of ~560–700 cm^{-1}, which are characteristic of Fe–O stretching of Si–O–Fe bonds [43–46]. In the spectra of the MNPs synthesised in this work, there were shoulders at ~621 cm^{-1}, which may indicate the Fe–O–Si bond formation (Figure 1). As a result, we obtained MNPs-SiO_2 **3** and **4**, which were then modified with aminopropylsilane residues (APS) to obtain MNPs-SiO_2-APS **5** and **6**, respectively (Scheme 1). The Fe_3O_4:SiO_2 ratio in all the obtained MNPs, according to energy-dispersive X-ray spectroscopy (EDX) data, was ~67:33 wt.%, and it did not change during the modification (Table 1). During the SiO_2 coating of MNP **2**, PMIDA desorption was observed. As a result, only ~31% of PMIDA molecules remained on the MNP surface. Further functionalisation of the MNP surface with the APS and the peptide derivative, as well as their treatment with TFA (95%), did not lead to a significant change in the level of PMIDA in the nanoconjugates: ~30% of the amount initially loaded onto MNPs **2** remained on the nanoparticles (Table 1), as evidenced by the results of the phosphorus content analysis by EDX.

We have previously demonstrated the possibility of conjugating RGD peptide derivatives both with APS amino groups fixed directly on the Fe_3O_4 MNP surface [47] and on the SiO_2 coating of nanoparticles [48].

In this work, we performed covalent binding of the Arg(Pbf)GlyAsp(OBu^t)$_2$ (RGD) tripeptide to the SiO_2 surface via a PEG linker (Scheme 1). For this purpose, a novel PEG-containing derivative of the RGD peptide was synthesised in the work. Synthesis of the initial RGD peptide was carried out in accordance with [40,41]. During the synthesis, the functional groups of the peptide were blocked in such a way that they could be deblocked simultaneously at the last stage of the synthesis. Next, the RGD derivative was conjugated

with the bifunctional molecule of oligomeric PEG_{25}, containing an activated carboxyl group (Scheme 1).

The obtained PEG derivative was characterised with ^1H NMR, HRMS, and HPLC data (Figure S1). In addition to the broad bands at 555–557 cm^{-1} (Fe–O ν) and 1064–1066, and 954–956 cm^{-1} (Si–O ν), attributed to the core and shell materials, respectively (Figures 1, S2 and S3), the absorption bands typical for the peptide were observed in the FTIR spectra of MNPs-RGD **7**–**12**: 1734–1735 cm^{-1} (C=O ν, $COOBu^t$), 1624–1626 cm^{-1} (C=O ν (amide 1)), 1548–1556 cm^{-1} (NH δ, N–C=O ν (amide 2), –NH–C(NH)–NH– ν (guanidine group)), and 1448–1455, 1369–1371 cm^{-1} (C–N ν).

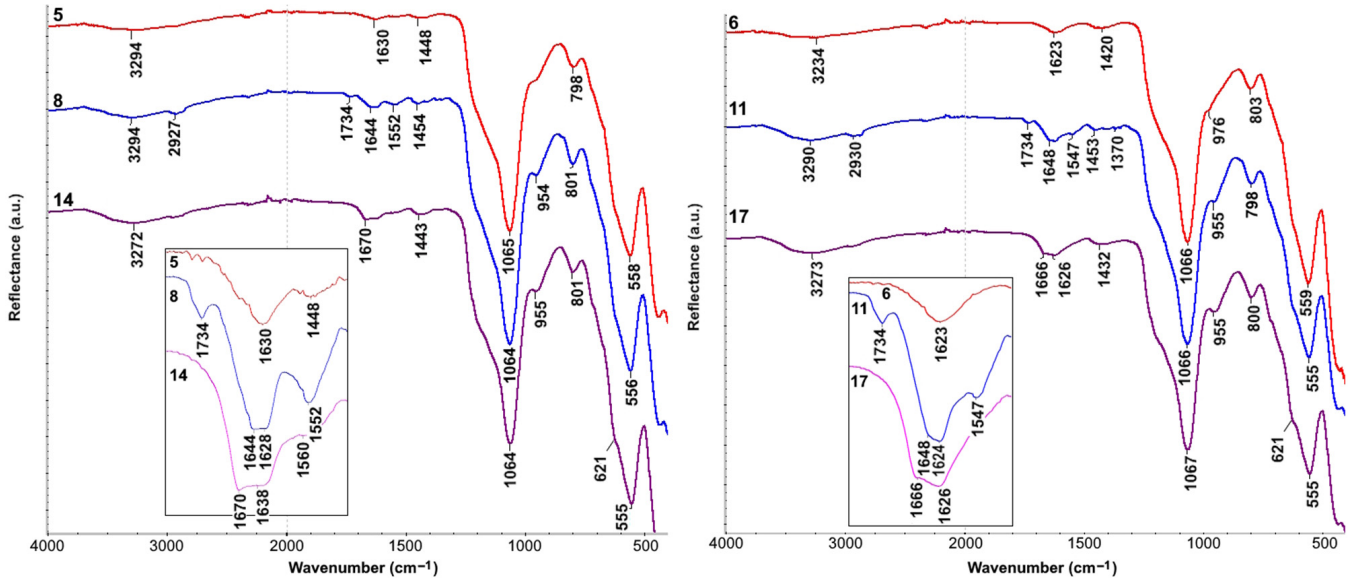

Figure 1. FTIR spectra of MNPs-SiO_2-APS **5** and **6** (red line), MNPs-RGD **8** and **11** (blue line), and MNPs-RGD*TFA **14** and **17** (purple line).

Table 1. Data on the chemical composition of synthesised nanoparticles.

MNP Type	MNP Number	Elemental Content, %				Content of Inorganic Components, %	Content of Organic Components, μmol/g	
		Fe [a]	Si [a]	P [a]	C [b]	Fe_3O_4:SiO_2 [c]	C_{PMIDA} [c]	$C_{PEG\text{-}RGD}$ [d]
MNPs	2	97.96 ± 0.16	0	2.04 ± 0.02	3.08 ± 0.01	-	413 ± 4	0
MNPs-SiO_2	3	77.90 ± 0.46	22.10 ± 0.10	0	-	69:31	0	0
	4	75.25 ± 0.09	24.09 ± 0.01	0.66 ± 0.04	1.62 ± 0.01	67:33	128 ± 9	0
MNPs-SiO_2-APS	5	76.57 ± 0.35	23.43 ± 0.10	0	1.84 ± 0.02	68:32	0	0
	6	74.88 ± 0.02	24.48 ± 0.04	0.64 ± 0.03	2.26 ± 0.04	66:34	124 ± 5	0
MNPs-RGD	7	74.90 ± 0.11	25.10 ± 0.41	0	3.81 ± 0.01	66:34	0	18.9 ± 0.3
	8	74.89 ± 0.11	25.11 ± 0.37	0	3.04 ± 0.04	66:34	0	11.4 ± 0.6
	9	73.28 ± 0.12	26.72 ± 0.35	0	2.73 ± 0.02	64:36	0	8.5 ± 0.4
	10	74.00 ± 0.12	25.38 ± 0.07	0.62 ± 0.02	4.78 ± 0.04	65:35	115 ± 4	24.2 ± 0.8
	11	74.06 ± 0.12	24.86 ± 0.13	0.65 ± 0.04	3.91 ± 0.08	66:34	124 ± 6	15.8 ± 1.2
	12	75.03 ± 0.12	24.33 ± 0.12	0.64 ± 0.03	3.44 ± 0.08	67:33	122 ± 6	11.3 ± 1.2
MNPs-RGD*TFA	13	76.86 ± 0.14	23.14 ± 0.22	0	3.81 ± 0.03	68:32	0	20.9 ± 0.6
	14	76.35 ± 0.14	23.65 ± 0.23	0	3.37 ± 0.04	68:32	0	16.2 ± 0.7
	15	76.86 ± 0.13	23.14 ± 0.32	0	2.81 ± 0.37	68:32	0	10.3 ± 4.1
	16	73.59 ± 0.12	25.75 ± 0.07	0.66 ± 0.07	4.72 ± 0.10	65:35	123 ± 13	26.2 ± 1.5
	17	75.32 ± 0.13	24.08 ± 0.07	0.60 ± 0.06	3.83 ± 0.01	67:33	115 ± 11	16.7 ± 0.5
	18	76.16 ± 0.16	23.31 ± 0.10	0.53 ± 0.04	3.88 ± 0.14	68:32	102 ± 7	17.3 ± 2.0

[a] Received as a result of EDX analysis. [b] Received as a result of CHN elemental analysis. [c] EDX data-based assessment. [d] CHN elemental analysis data-based assessment.

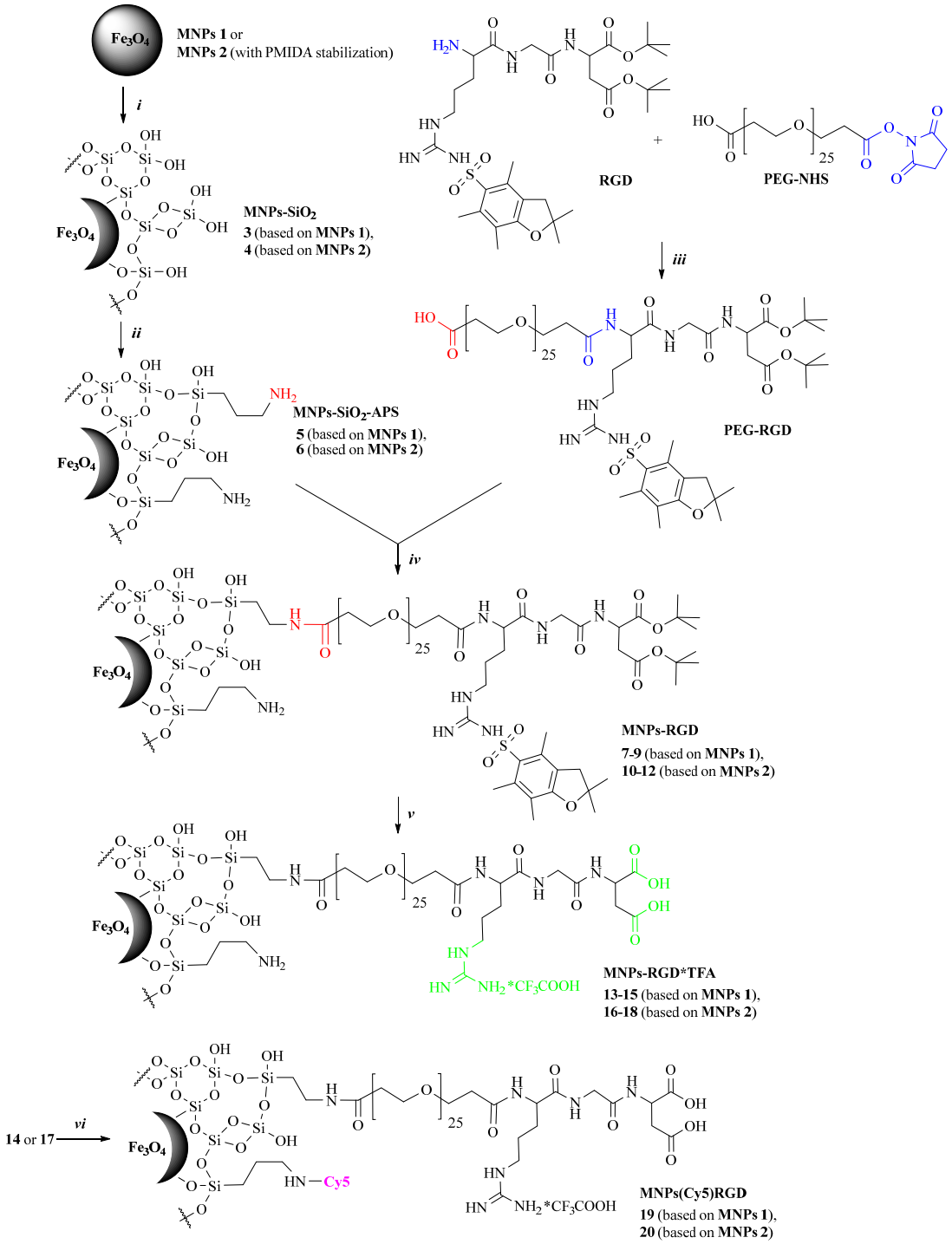

Scheme 1. Surface modification of MNPs with the RGD-PEG nanoconjugate.

The presence of a free carboxyl group in the PEG molecule further allowed conjugation of the PEG-derived RGD peptide (PEG-RGD) with MNPs-SiO_2-APS (**5** and **6**) using the condensing agent HBTU (Scheme 1). To optimise the synthesis, condensation was carried out at a ratio of MNPs-SiO_2-APS:PEG-RGD of 2:1, 5:1, or 10:1, and MNPs-RGD **7–9** and **10–12** were obtained, respectively. Simultaneous removal of Bu^t and Pbf groups was carried out in a TFA medium [49,50], and MNPs-RGD*TFA **13–15** and **16–18** with the free guanidine group of L-Arg and carboxyl groups of L-Asp were obtained, respectively (Scheme 1). The

presence of the RGD peptide was qualitatively confirmed by FTIR spectroscopy data. As an example, the FTIR spectra of MNPs-RGD **8** and **11** and MNPs-RGD*TFA **14** and **17** are demonstrated in Figure 1.

As can be observed, in the region of 1800–1485 cm^{-1}, the intensity of the bands attributed to the RGD peptide decreased for conjugates obtained using lower amounts of PEG-RGD (Figures S2 and S3). For MNPs-RGD **10**–**12** obtained on the basis of PMIDA-stabilised MNPs, the intensity of the bands characteristic of the peptide was higher than for MNPs-RGD **7**–**9**. After treatment of MNPs-RGD **7**–**12** with TFA, the bands at ~1730 cm^{-1} ($COOBu^t$) in the spectra of MNPs-RGD*TFA **13**–**18** disappeared, but additional bands appeared at 1670 cm^{-1} (COOH), which may indicate deblocking of the L-Asp carboxyl groups (Figures 1 and S4). The amount of PEG-RGD in the corresponding MNPs-RGD **7**–**12** was calculated using the CHN elemental analysis and EDX data (Table 1), in accordance with [8,47,48]. An increase in the MNPs-SiO_2-APS:PEG-RGD ratio naturally led to a decrease in the amount of peptide in the resulting MNPs. It was shown that MNPs-RGD **10**–**12** obtained using PMIDA contained large amounts of peptide. The same trends were observed for MNPs-RGD*TFA **13**–**18**.

As an example, TEM images, size distributions (with statistical data), as well as electron diffraction patterns of two types of nanoparticles, MNPs-RGD*TFA **14** and **17**, are shown in Figure 2. According to TEM data, the average size of the MNPs obtained was ~12 nm. The core diameter was 9.3 nm (standard deviation 1.9 and median 8.9 nm). The magnetite structure was confirmed by electron diffraction data (card mp-19306, materialsproject.org (accessed on 21 November 2024); Figure 2c,f).

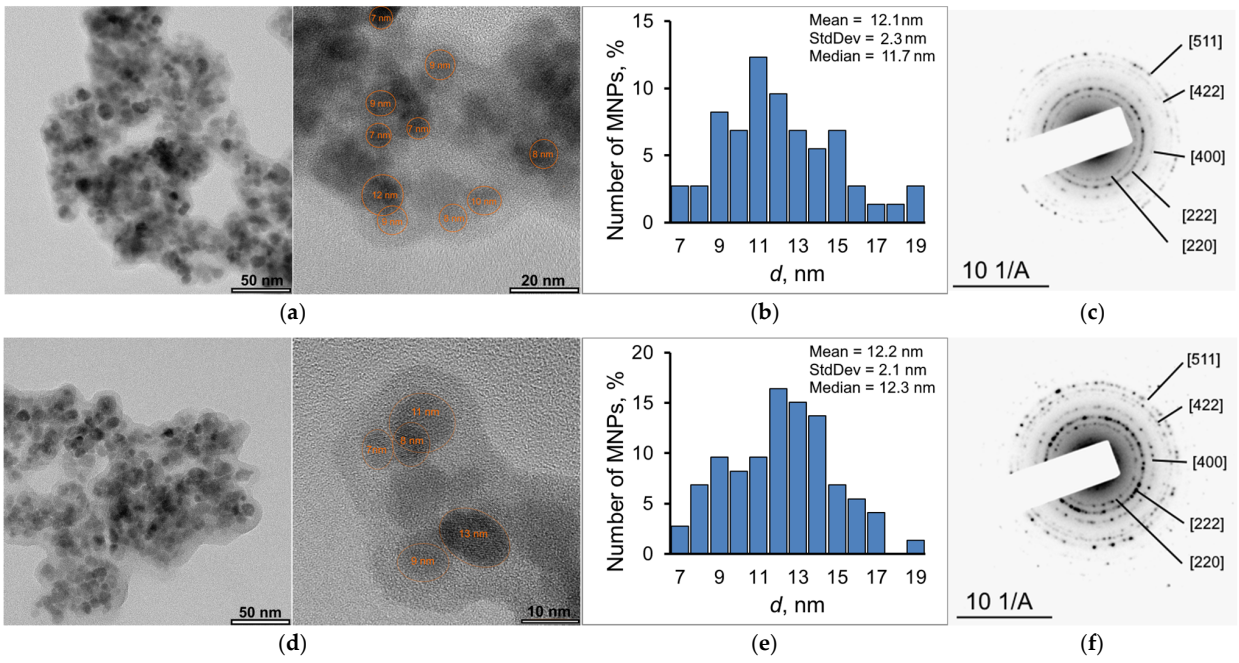

Figure 2. TEM images of MNPs-RGD*TFA **14** (**a**) and **17** (**d**), their size distributions (**b**,**e**), as well as their electron diffraction patterns (**c**,**f**), correspondingly.

The materials had pronounced magnetic properties, so the saturation magnetisation, *M*s, of MNPs-RGD **8** and **11** was 42 and 28 emu/g (coercivity *H*c < 1 Oe), correspondingly (Figure 3a).

As is known, the parameter characterising the ability of magnetic materials to exhibit MR contrast properties is relaxivity (*r*2 and *r*1). The relaxivity *r*2 values of colloidal solutions of MNPs-RGD*TFA **14** and **17** were 204 and 200 $mmol^{-1}$ s^{-1}, respectively (Figure 3b,c), and were higher than the *r*2 values characteristic of most commercially available drugs (~100 $mmol^{-1}$ s^{-1}) [51–53]. This indicates that these materials can be used as *T*2-contrast agents.

MNPs-RGD **7**–**12** rapidly aggregated in an aqueous medium, but after removal of the protective groups from RGD residues, the nanoparticles yielded stable colloidal solutions (Table 2). Colloidal solutions of MNPs-RGD*TFA **16**–**18** had slightly better hydrodynamic characteristics than solutions of MNPs-RGD*TFA **13**–**15**, which emphasised the stabilising role of PMIDA molecules.

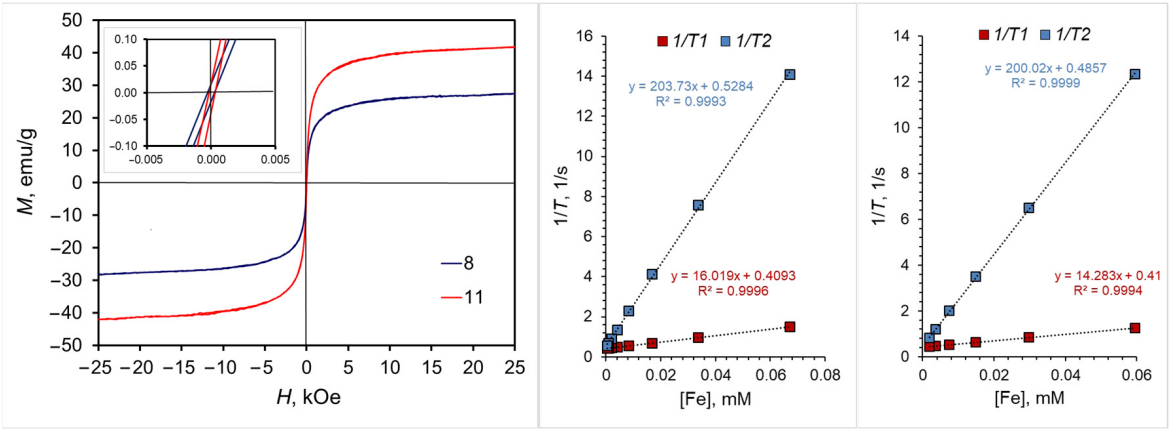

(**a**) (**b**) (**c**)

Figure 3. (**a**) Magnetisation curves of MNPs-RGD **8** and **11**. Relaxivities *r*1 and *r*2 for MNPs-RGD*TFA (**b**) **14** and (**c**) **17**.

Table 2. DLS data.

MNPs-RGD*TFA	DLS Data	
	D_h, nm	PdI
13	80	0.2
14	114	0.25
15	112	0.21
16	84	0.21
17	82	0.27
18	82	0.26

This research demonstrated the possibility of introducing a fluorescent label into the MNPs, using Cyanine5 as an example. It was introduced at the last stage of the synthesis by condensation of free amino groups of APS with the activated ester of Cyanine5-NHS, resulting in MNPs(Cy5)RGD **19** and **20**, correspondingly (Scheme 1). For biological experiments, PEG-modified MNPs (MNPs(Cy5)PEG) **21** and **22** (based on MNPs **5** and **6**, correspondingly) labelled with Cyanine5 of a similar structure, but not containing the RGD fragment (Scheme 2), were additionally synthesised. The emission spectra of the obtained nanoconjugates **19**–**22** corresponded to the spectra of the Cyanine5 dye (Figure S5).

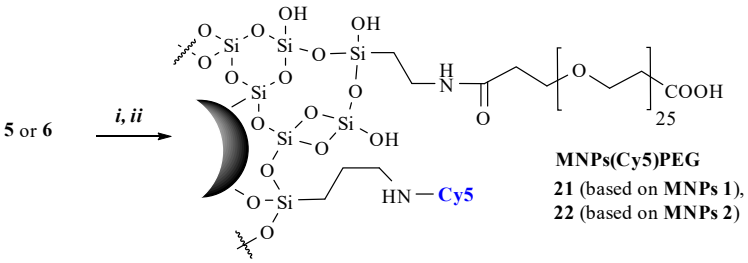

i: PEG-NHS, CH_2Cl_2 dry, 20 h; ***ii***: Cy5-NHS, MeCN, 20 h.

Scheme 2. Synthesis of Fe_3O_4 MNP conjugates with PEG.

3.2. In Vitro Experiments

For the synthesised nanoconjugates **19**–**22**, cytotoxicity (MTT test [54]) was determined on the 4T1 and MDA-MB231 tumour cell lines (Figures S6 and S7). In general, the MNPs decreased cell viability, and in most cases, the cytotoxic effect increased from 24 to 48 h (at 48 h, the proportion of viable cells was about 50% of the initial number).

It Is noteworthy that the cytotoxicity of MNPs depended on the cell type. Thus, for the 4T1 cell line, toxicity reached ~50% at the highest concentrations of MNPs. However, for the human cell line MDA-MB231, toxicity did not exceed 70%, which allowed us to consider MNPs as generally non-toxic [55]. The adverse effect on cell viability may be explained by the ability of MNPs Fe_3O_4 to induce the reactive oxygen species production in cells [48]. Also, the ability of RGD derivatives to exhibit cytotoxicity against tumour cell lines is well known (for example, Cilengitide (c(RGDf-N(Me)K), which is used to treat glioblastoma [56]).

Effective uptake of the MNPs(Cy5)RGD **19** and **20** by MDA-MB231 cells was demonstrated by flow cytometry (Figure 4). Already after 4 h of incubation with 1.25 μg/mL of MNPs, more than 99.5% of the cells were positive for Cy5 in all samples tested.

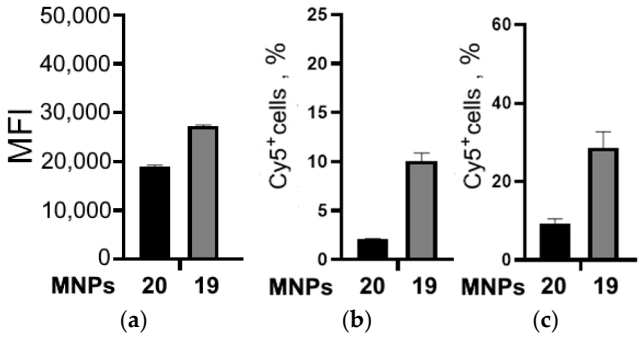

Figure 4. MNPs(Cy5)RGD **19** and **20** uptake efficiency by MDA-MB231 cells incubated in (**a**) complete medium at 37 °C for 4 h (the OY axis shows the fluorescence intensity because the number of $Cy5^+$ cells was ~100%), (**b**) complete medium for 1 h on ice, removing MNPs, and then left at 37 °C for 4 h, and (**c**) DMEM/F12 for 1 h on ice, removing MNPs, and then left at 37 °C for 4 h (in figures (**b**,**c**), the OY axis shows the % of $Cy5^+$ cells). Data are provided as mean ± SD, $n = 4$.

To assess the penetration of MNPs(Cy5)RGD into cells via specific binding to surface receptors, the MNPs were added to pre-chilled cells and incubated for 1 h on ice (4 °C) to suppress the uptake of MNPs via nonspecific endocytosis. After incubation, unbounded nanoparticles were removed, and cells were held at 37 °C for 4 h to complete the endocytosis of MNPs bonded to surface receptors. As a result, it was demonstrated that the percentage of cells containing MNPs(Cy5)RGD **19** and **20** was 29 and 9%, respectively. In the presence of serum, the efficiency of MNPs' uptake decreased and amounted to 10% of cells for **19** and 2% for **20**. The observed effect can be attributed to the formation of a protein corona on the nanoparticles' surfaces [37,57–59]. This can be explained either by the effect of PMIDA on the formation of a protein corona around the particles and increased shielding of the RGD peptide, or by the size effect of MNPs. In the case of PMIDA-stabilised MNP **20**, serum proteins were likely to be adsorbed onto the MNP surface and, accordingly, shielded the RGD peptides to a greater extent than in the case of MNP **19**. This led to significant reduction of MNPs' interaction with cell surface receptors. On the other hand, the hydrodynamic size of MNP **20** obtained using PMIDA was smaller (D_h 91 nm and PdI 0.14) than the diameter of MNP **19** obtained using bare MNPs (D_h 144 nm and PdI 0.27). It is possible that cells endocytosed larger MNPs to a greater extent. Thus, in this case, the size effect played a predominant role in the process of MNPs' uptake by cells.

Penetration of MNPs(Cy5)RGD **19** and **20** into MDA-MB231 and 4T1 cell lines was demonstrated by fluorescence microscopy (Figure 5).

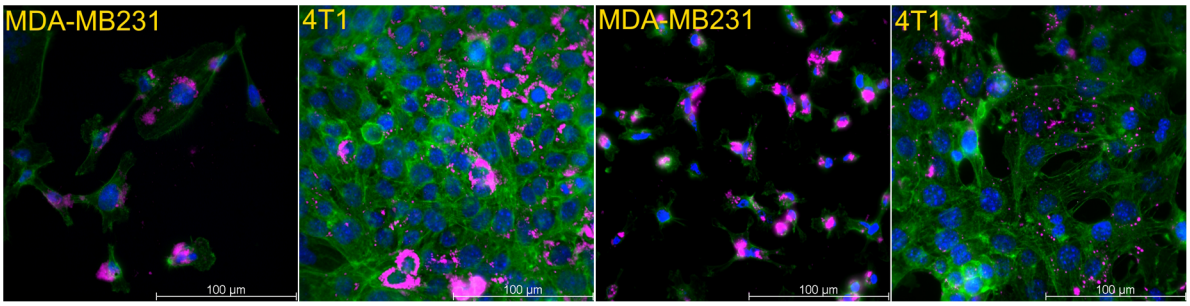

(**a**) (**b**) (**c**) (**d**)

Figure 5. Fluorescence microscopy images of cells (MDA-MB231 and 4T1) after being held with MNPs(Cy5)RGD **19** (**a**,**b**) and **20** (**c**,**d**) in complete DMEM/F12 for 1 h on ice, removal of MNPs, followed by being held at 37 °C for 24 h. Actin fibres of the cells are green (Phalloidin Atto 488), nuclei are blue (DAPI), and MNPs are magenta (Cy5).

4. Conclusions

As a result, a convenient approach to obtaining SiO_2/PEG-coated MNPs conjugated with the targeting RGD peptide and Cy5 fluorescent label was proposed. The use of PMIDA-stabilised MNPs can make it possible to obtain MNPs with better hydrodynamic characteristics and with a higher peptide content, in comparison with non-stabilised MNPs. Using MDA-MB231 cells as an example, the ability of the MNPs(Cy5)RGD to internalise the cells was demonstrated. The cellular uptake was more efficient for nanoconjugates obtained without PMIDA. Nevertheless, the MNP accumulation in cells occurred mainly due to nonspecific endocytosis. The formation of a protein corona around the MNPs(Cy5)RGD reduced the efficiency of their cellular uptake. The data obtained can be used in the development of nanomaterials for diagnostics and targeted therapy of oncological diseases, as well as for labelling and visualisation of tumour cells.

Supplementary Materials: The following supporting information can be downloaded at: https://www.mdpi.com/article/10.3390/jcs8120486/s1. Figure S1. (a) 1H NMR, (b) MS spectra of PEG-RGD conjugate and (c) HPLC of PEG-RGD conjugate; Figure S2. FT-IR spectra of MNPs-SiO_2 3, MNPs-APS 5 and MNPs-RGD 7–9; Figure S3. FT-IR spectra of MNPs 2, MNPs-SiO_2 4, MNPs-APS 6 and MNPs-RGD 10–12; Figure S4. FT-IR spectra of MNPs-RGD*TFA 13–18; Figure S5. Excitation (1) and emission (2) spectra of MNPs 19 (a), 20 (b), 21 (c) and 22 (d), respectively; Figure S6. Evaluation of the viability of 4T1 and MDA-MB231 cells by the MTT test after incubation with MNPs 19 and 21 for 24 and 48 h; Figure S7. Evaluation of the viability of 4T1 and MDA-MB231 cells by the MTT test after incubation with MNPs 20 and 22 for 24 and 48 h.

Author Contributions: Conceptualisation, A.M.D.; methodology, A.M.D. and A.G.P.; investigation, A.M.D., A.V.V., A.G.P., A.A.S., L.V.E., M.S.K., M.A.U., I.V.B. and A.S.M.; writing—original draft preparation, A.M.D.; writing—review and editing, V.P.K. and A.G.P.; visualisation, A.M.D.; supervision, V.P.K. All authors have read and agreed to the published version of the manuscript.

Funding: This research received no funding.

Data Availability Statement: The original contributions presented in the study are included in the article/Supplementary Material. Further inquiries can be directed to the corresponding authors.

Acknowledgments: The study was carried out with the support of the state assignment of IOS UB RAS (Theme No. 124020500044-4 (in part of nanocomposite synthesis and analysis), No. 124020500023-9 (in part of RGD conjugate synthesis) and (in part of organic compounds analysis by ^{1}H NMR, HRMS and RP-HPLC)). The equipment of the Centre for Joint Use "Spectroscopy and Analysis of Organic Compounds" at the Postovsky Institute of Organic Synthesis and Ural Centre for Shared Use "Modern Nanotechnology" at the Ural Federal University were used. The research of magnetic properties and relaxivity was carried out within the state assignment "Magnit" No. 122021000034-9.

Conflicts of Interest: The authors declare no conflicts of interest.

References

1. Li, F.; Qin, Y.; Lee, J.; Liao, H.; Wang, N.; Davis, T.P.; Qiao, R.; Ling, D. Stimuli-responsive nano-assemblies for remotely controlled drug delivery. *J. Control. Release* **2020**, *322*, 566–592. [CrossRef]
2. Mohapatra, J.; Nigam, S.; George, J.; Arellano, A.C.; Wang, P.; Liu, J.P. Principles and applications of magnetic nanomaterials in magnetically guided bioimaging. *Mater. Today Phys.* **2023**, *32*, 101003. [CrossRef]
3. Shabatina, T.I.; Vernaya, O.I.; Shimanovskiy, N.L.; Melnikov, M.Y. Metal and metal oxides nanoparticles and nanosystems in anticancer and antiviral theragnostic agents. *Pharmaceutics* **2023**, *15*, 1181. [CrossRef] [PubMed]
4. Shen, L.; Li, B.; Qiao, Y. Fe_3O_4 Nanoparticles in targeted drug/gene delivery systems. *Materials* **2018**, *11*, 324. [CrossRef] [PubMed]
5. Kurczewska, J.; Dobosz, B. Recent progress and challenges regarding magnetite-based nanoparticles for targeted drug delivery. *Appl. Sci.* **2024**, *14*, 1132. [CrossRef]
6. Chen, X.; Wang, H.; Shi, J.; Chen, Z.; Wang, Y.; Gu, S.; Fu, Y.; Huang, J.; Ding, J.; Yu, L. An injectable and active hydrogel induces mutually enhanced mild magnetic hyperthermia and ferroptosis. *Biomaterials* **2023**, *298*, 122139. [CrossRef] [PubMed]
7. Gupta, R.; Kaur, T.; Chauhan, A.; Kumar, R.; Kuanr, B.K.; Sharma, D. Tailoring nanoparticles design for enhanced heating efficiency and improved magneto-chemo therapy for glioblastoma. *Biomater. Adv.* **2022**, *139*, 213021. [CrossRef]
8. Demin, A.M.; Vakhrushev, A.V.; Pershina, A.G.; Valova, M.S.; Efimova, L.V.; Syomchina, A.A.; Uimin, M.A.; Minin, A.S.; Levit, G.L.; Krasnov, V.P.; et al. Magnetic-responsive doxorubicin-containing materials based on Fe_3O_4 nanoparticles with a SiO_2/PEG shell and study of their effects on cancer cell lines. *Int. J. Mol. Sci.* **2022**, *23*, 9093. [CrossRef]
9. Shen, B.; Ma, Y.; Yu, S.; Ji, C. Smart multifunctional magnetic nanoparticle-based drug delivery system for cancer thermo-chemotherapy and intracellular imaging. *ACS Appl. Mater. Interfaces* **2016**, *8*, 24502–24508. [CrossRef]
10. Li, Z.; Bai, R.; Yi, J.; Zhou, H.; Xian, J.; Chen, C. Designing smart iron oxide nanoparticles for MR imaging of tumors. *Chem. Biomed. Imaging* **2023**, *1*, 315–339. [CrossRef]
11. Chen, C.; Huang, B.; Zhang, R.; Sun, C.; Chen, L.; Ge, J.; Zhou, D.; Li, Y.; Wu, S.; Qian, Z.; et al. Surface ligand-regulated renal clearance of MRI/SPECT dual-modality nanoprobes for tumor imaging. *J. Nanobiotechnol.* **2024**, *22*, 245. [CrossRef]
12. Demin, A.M.; Pershina, A.G.; Minin, A.S.; Brikunova, O.Y.; Murzakaev, A.M.; Perekucha, N.A.; Romashchenko, A.V.; Shevelev, O.B.; Uimin, M.A.; Byzov, I.V.; et al. Smart design of pH-responsive system based on pHLIP-modified magnetite nanoparticles for tumor MRI. *ACS Appl. Mater. Interfaces* **2021**, *13*, 36800. [CrossRef] [PubMed]
13. Pershina, A.G.; Brikunova, O.Y.; Demin, A.M.; Abakumov, M.A.; Vaneev, A.N.; Naumenko, V.A.; Erofeev, A.S.; Gorelkin, P.V.; Nizamov, T.R.; Muslimov, A.R.; et al. Variation in tumor pH affects pH-triggered delivery of peptide-modified magnetic nanoparticles. *Nanomed. Nanotechnol. Biol. Med.* **2021**, *32*, 102317–102329. [CrossRef] [PubMed]
14. Shrestha, S.; Banstola, A.; Jeong, J.-H.; Seo, J.H.; Yook, S. Targeting Cancer Stem Cells: Therapeutic and diagnostic strategies by the virtue of nanoparticles. *J. Control. Release* **2022**, *348*, 518–536. [CrossRef] [PubMed]
15. Yan, S.; Hu, K.; Zhang, M.; Sheng, J.; Xu, X.; Tang, S.; Li, Y.; Yang, S.; Si, G.; Mao, Y.; et al. Extracellular magnetic labeling of biomimetic hydrogel-induced human mesenchymal stem cell spheroids with ferumoxytol for MRI tracking. *Bioact. Mater.* **2023**, *19*, 418–428. [CrossRef] [PubMed]
16. Demin, A.M.; Mekhaev, A.V.; Kandarakov, O.F.; Popenko, V.I.; Leonova, O.G.; Murzakaev, A.M.; Kuznetsov, D.K.; Uimin, M.A.; Minin, A.S.; Shur, V.Y.; et al. L-Lysine-modified Fe_3O_4 nanoparticles for magnetic cell labelling. *Colloids Surf. B Biointerfaces* **2020**, *190*, 110879. [CrossRef]
17. Frenea-Robin, M.; Marchalot, J. Basic principles and recent advances in magnetic cell separation. *Magnetochemistry* **2022**, *8*, 11. [CrossRef]
18. Polyakova, N.; Kandarakov, O.; Belyavsky, A. Selection of cell populations with high or low surface marker expression using magnetic sorting. *Cells* **2023**, *12*, 1286. [CrossRef] [PubMed]
19. Savvateeva, M.V.; Demin, A.M.; Krasnov, V.P.; Belyavsky, A.V. Magnetic stromal layers for enhanced and unbiased recovery of co-cultured hematopoietic cells. *Anal. Biochem.* **2016**, *509*, 146–155. [CrossRef]
20. Duan, X.; Wang, P.; He, L.; He, Z.; Wang, S.; Yang, F.; Gao, C.; Ren, W.; Lin, J.; Chen, T.; et al. Peptide-functionalized inorganic oxide nanomaterials for solid cancer imaging and therapy. *Adv. Mater.* **2024**, *23*, 11548. [CrossRef]
21. David, H.; Oryani, M.A.; Rezagholinejad, N.; Esparham, A.; Tajaldini, M.; Karimi-Shahri, M. RGD peptide in cancer targeting: Benefits, challenges, solutions, and possible integrin–RGD interactions. *Cancer Med.* **2024**, *13*, e6800. [CrossRef]
22. Qin, W.; Chandra, J.; Abourehab, M.A.S.; Gupta, N.; Chen, Z.-S.; Kesharwani, P.; Cao, H.-L. New opportunities for RGD-engineered metal nanoparticles in cancer. *Mol. Cancer* **2023**, *22*, 87. [CrossRef] [PubMed]
23. Arriortua, C.O.K.; Insausti, M.; Lezama, L.; de Muro, I.G.; Garaio, E.; de la Fuente, J.M.; Fratila, R.M.; Morales, M.P.; Costa, R.; Eceiza, M.; et al. RGD-Functionalized Fe_3O_4 nanoparticles for magnetic hyperthermia. *Colloids Surf. B* **2018**, *165*, 315–324. [CrossRef] [PubMed]
24. Luo, Y.; Yang, J.; Yan, Y.; Li, J.; Shen, M.; Zhang, G.; Mignani, S.; Shi, X. RGD-functionalized ultrasmall iron oxide nanoparticles for targeted T_1-weighted MR imaging of gliomas. *Nanoscale* **2015**, *7*, 14538–14546. [CrossRef]
25. Zhang, C.; Jugold, M.; Woenne, E.C.; Lammers, T.; Morgenstern, B.; Mueller, M.M.; Zentgraf, H.; Bock, M.; Eisenhut, M.; Semmler, W.; et al. Specific targeting of tumor angiogenesis by RGD-conjugated ultrasmall superparamagnetic iron oxide particles using a clinical 1.5-T magnetic resonance scanner. *Cancer Res.* **2007**, *67*, 1555–1562. [CrossRef]
26. Zheng, S.W.; Huang, M.; Hong, R.Y.; Deng, S.M.; Cheng, L.F.; Gao, B.; Badami, D. RGD-conjugated iron oxide magnetic nanoparticles for magnetic resonance imaging contrast enhancement and hyperthermia. *J. Biomater. Appl.* **2014**, *28*, 1051–1059. [CrossRef]

27. Fernández-Barahona, I.; Gutiérrez, L.; Veintemillas-Verdaguer, S.; Pellico, J.; Morales, M.P.; Catala, M.; del Pozo, M.A.; Ruiz-Cabello, J.; Herranz, F. Cu-doped extremely small iron oxide nanoparticles with large longitudinal relaxivity: One-pot synthesis and in vivo targeted molecular imaging. *ACS Omega* **2019**, *4*, 2719–2727. [CrossRef]
28. Sani, S.; Messe, M.; Fuchs, Q.; Pierrevelcin, M.; Laquerriere, P.; Entz-Werle, N.; Reita, D.; Etienne-Selloum, N.; Bruban, V.; Choulier, L.; et al. Biological relevance of RGD-integrin subtype-specific ligands in cancer. *ChemBioChem* **2021**, *22*, 1151–1160. [CrossRef]
29. Ludwig, B.S.; Kessler, H.; Kossatz, S.; Reuning, U. RGD-binding integrins revisited: How recently discovered functions and novel synthetic ligands (re-)shape an ever-evolving field. *Cancers* **2021**, *13*, 1711. [CrossRef]
30. Liu, S. Radiolabeled cyclic RGD peptide bioconjugates as radiotracers targeting multiple integrins. *Bioconjug. Chem.* **2015**, *26*, 1413. [CrossRef]
31. Dong, X.; Yu, Y.; Wang, Q.; Xi, Y.; Liu, Y. Interaction mechanism and clustering among RGD peptides and integrins. *Mol. Inf.* **2017**, *36*, 1600069. [CrossRef] [PubMed]
32. Sapsford, K.E.; Algar, W.R.; Berti, L.; Gemmill, K.B.; Casey, B.J.; Oh, E.; Stewart, M.H.; Medintz, I.L. Functionalizing nanoparticles with biological molecules: Developing chemistries that facilitate nanotechnology. *Chem. Rev.* **2013**, *113*, 1904–2074. [CrossRef] [PubMed]
33. Gao, Z.; Hou, Y.; Zeng, J.; Chen, L.; Liu, C.; Yang, W.; Gao, M. Tumor microenvironment-triggered aggregation of anti-phagocytosis ^{99m}Tc-labelled Fe_3O_4 nanoprobes for enhanced tumor imaging in vivo. *Adv. Mater.* **2017**, *29*, 1701095. [CrossRef] [PubMed]
34. Tsiapa, I.; Efthimiadou, E.K.; Fragogeorgi, E.; Loudos, G.; Varvarigou, A.D.; Bouziotis, P.; Kordas, G.C.; Mihailidis, D.; Nikiforidis, G.C.; Xanthopoulos, S.; et al. ^{99m}Tc-labeled aminosilane-coated iron oxide nanoparticles for molecular imaging of $\alpha_V\beta_3$-mediated tumor expression and feasibility for hyperthermia treatment. *J. Colloid Interface Sci.* **2014**, *433*, 163–175. [CrossRef]
35. Liolios, C.; Koutsikou, T.S.; Salvanou, E.-A.; Kapiris, F.; Machairas, E.; Stampolaki, M.; Kolocouris, A.; Efthimiadou, E.K.; Bouziotis, P. Synthesis and in vitro proof-of-concept studies on bispecific iron oxide magnetic nanoparticles targeting PSMA and GRP receptors for PET/MR imaging of prostate cancer. *Int. J. Pharm.* **2022**, *624*, 122008. [CrossRef]
36. Demin, A.M.; Maksimovskikh, A.V.; Mekhaev, A.V.; Kuznetsov, D.K.; Minin, A.S.; Pershina, A.G.; Uimin, M.A.; Shur, V.Y.; Krasnov, V.P. Silica coating of Fe_3O_4 magnetic nanoparticles with PMIDA assistance to increase the surface area and enhance peptide immobilization efficiency. *Ceram. Int.* **2021**, *47*, 23078–23087. [CrossRef]
37. Pershina, A.G.; Demin, A.M.; Perekucha, N.A.; Brikunova, O.Y.; Efimova, L.V.; Nevskaya, K.V.; Vakhrushev, A.V.; Zgoda, V.G.; Uimin, M.A.; Minin, A.S.; et al. Peptide ligands on the PEGylated nanoparticle surface and human serum composition are key factors for the interaction between immune cells and nanoparticles. *Colloids Surf. B* **2023**, *221*, 112981. [CrossRef]
38. Zhang, X.; Wang, H.; Ma, Z.; Wu, B. Effects of pharmaceutical PEGylation on drug metabolism and its clinical concerns. *Expert Opin. Drug Metab. Toxicol.* **2014**, *10*, 1691–1702. [CrossRef]
39. Padín-González, E.; Lancaster, P.; Bottini, M.; Gasco, P.; Tran, L.; Fadeel, B.; Wilkins, T.; Monopoli, M.P. Understanding the role and impact of poly(ethylene glycol) (PEG) on nanoparticle formulation: Implications for COVID-19 vaccines. *Front. Bioeng. Biotechnol.* **2022**, *10*, 882363. [CrossRef]
40. Vigorov, A.Y.; Demin, A.M.; Nizova, I.A.; Krasnov, V.P. Synthesis of derivatives of the RGD peptide with the residues of glutaric and adipic acids. *Russ. J. Bioorg. Chem.* **2014**, *40*, 142–150. [CrossRef]
41. Gruzdev, D.A.; Vakhrushev, A.V.; Demin, A.M.; Baryshnikova, M.A.; Levit, G.L.; Krasnov, V.P.; Charushin, V.N. Synthesis of *closo*- and *nido*-carborane derivatives of the KRGD peptide. *J. Organomet. Chem.* **2024**, *1008*, 123052. [CrossRef]
42. Gueddida, S.; Badawi, M.; Lebègue, S. Grafting of iron on amorphous silica surfaces from ab initio calculations. *J. Chem. Phys.* **2020**, *152*, 214706. [CrossRef] [PubMed]
43. Ahangaran, F.; Hassanzadeh, A.; Nouri, S. Surface modification of Fe_3O_4@SiO_2 microsphere by silane coupling agent. *Int. Nano Lett.* **2013**, *3*, 23. [CrossRef]
44. Fang, G.; Chen, H.; Zhang, Y.; Chen, A. Immobilization of pectinase onto Fe_3O_4@SiO_2–NH_2 and its activityand stability. *Int. J. Biol. Macromol.* **2016**, *88*, 189–195. [CrossRef] [PubMed]
45. Khummalai, N.; Boonamnuayvitaya, V. Suppression of arsenopyrite surface oxidation by sol-gel coatings. *Biosci. Bioeng.* **2005**, *99*, 277–284. [CrossRef] [PubMed]
46. Yang, S.; Luo, T.; Fan, J.; Zhou, C.; Hu, M.; Wang, J.; Wen, L.; Qin, L.; Liu, G. Performance and mechanisms of PropS-SH/HA coatings in the inhibition of pyrite oxidation. *ACS Omega* **2021**, *6*, 32011–32021. [CrossRef]
47. Demin, A.M.; Vigorov, A.Y.; Nizova, I.A.; Uimin, M.A.; Shchegoleva, N.N.; Ermakov, A.E.; Krasnov, V.P.; Charushin, V.N. Functionalization of Fe_3O_4 magnetic nanoparticles with RGD peptide derivatives. *Mendeleev Commun.* **2014**, *24*, 20–22. [CrossRef]
48. Demin, A.M.; Vakhrushev, A.V.; Mekhaev, A.V.; Uimin, M.A.; Krasnov, V.P. Modification of Fe_3O_4 magnetic nanoparticles with a GRGD peptide. *Russ. Chem. Bull.* **2021**, *70*, 449–456. [CrossRef]
49. Carpino, L.A.; Shroff, H.; Triolo, S.A.; Mansour, E.-S.M.E.; Wenschuh, H.; Albericio, F. The 2,2,4,6,7-pentamethyldihydrobenzofuran-5-sulfonyl group (Pbf) as arginine side chain protectant. *Tetrahedron Lett.* **1993**, *34*, 7829. [CrossRef]
50. Varshney, R.; Hazari, P.P.; Uppal, J.K.; Pal, S.; Stromberg, R.; Allard, M.; Mishra, A.K. Solid phase synthesis, radiolabeling and biological evaluation of a ^{99m}Tc-labeled αVβ3 tripeptide (RGD) conjugated to DOTA as a tumor imaging agent. *Cancer Biol. Ther.* **2011**, *11*, 893–901. [CrossRef]
51. Wang, Y.X. Superparamagnetic iron oxide based MRI contrast agents: Current status of clinical application. *Quant. Imaging Med. Surg.* **2011**, *1*, 35–40. [CrossRef] [PubMed]

52. Estelrich, J.; Sánchez-Martín, M.J.; Busquets, M.A. Nanoparticles in magnetic resonance imaging: From simple to dual contrast agents. *Int. J. Nanomed.* **2015**, *10*, 1727–1741. [CrossRef]
53. Tegafaw, T.; Liu, S.; Ahmad, M.Y.; Saidi, A.K.A.A.; Zhao, D.; Liu, Y.; Nam, S.-W.; Chang, Y.; Lee, G.H. Magnetic nanoparticle-based high-performance positive and negative magnetic resonance imaging contrast agents. *Pharmaceutics* **2023**, *15*, 1745. [CrossRef] [PubMed]
54. Mosmann, T. Rapid colorimetric assay for cellular growth and survival: Application to proliferation and cytotoxicity assays. *J. Immunol. Methods* **1983**, *65*, 55–63. [CrossRef] [PubMed]
55. *ISO-10993-5*; Biological Evaluation of Medical Devices Part 5: Test for Cytotoxicity: In Vitro Methods. ANSI/AAMI: Arlington, VA, USA, 1999.
56. Dechantsreiter, M.A.; Planker, E.; Mathä, B.; Lohof, E.; Hölzemann, G.; Jonczyk, A.; Goodman, S.L.; Kessler, H. N-Methylated cyclic RGD peptides as highly active and selective $\alpha_V\beta_3$ integrin antagonists. *J. Med. Chem.* **1999**, *42*, 3033–3040. [CrossRef]
57. Pershina, A.G.; Efimova, L.V.; Brikunova, O.Y.; Nevskaya, K.V.; Sukhinina, E.V.; Hmelevskaya, E.S.; Demin, A.M.; Naumenko, V.A.; Malkeyeva, D.; Kiseleva, E.; et al. Nano-bio interaction of magnetic nanoparticles with cells in a tumor at the single-cell level. *Nano Today* **2024**, *56*, 102300. [CrossRef]
58. Salvati, A.; Pitek, A.S.; Monopoli, M.P.; Prapainop, K.; Bombelli, F.B.; Hristov, D.R.; Kelly, P.M.; Åberg, C.; Mahon, E.; Dawson, K.A. Transferrin-functionalized nanoparticles lose their targeting capabilities when a biomolecule corona adsorbs on the surface. *Nat. Nanotechnol.* **2013**, *8*, 137–143. [CrossRef]
59. Portilla, Y.; Mulens-Arias, V.; Daviu, N.; Paradela, A.; Perez-Yagüe, S.; Barber, D.F. Interaction of iron oxide nanoparticles with macrophages is influenced distinctly by "Self" and "Non-Self" biological identities. *ACS Appl. Mater. Interfaces* **2023**, *15*, 35906–35926. [CrossRef]